Study of the structure and dynamics of poly(vinyl pyrrolidone) by molecular dynamics simulations validated by quasielastic neutron scattering and x-ray diffraction experiments

Rémi Busselez, Arantxa Arbe, Fernando Alvarez, Juan Colmenero, and Bernhard Frick

Citation: The Journal of Chemical Physics **134**, 054904 (2011); doi: 10.1063/1.3533771
View online: https://doi.org/10.1063/1.3533771
View Table of Contents: http://aip.scitation.org/toc/jcp/134/5
Published by the American Institute of Physics

Study of the structure and dynamics of poly(vinyl pyrrolidone) by molecular dynamics simulations validated by quasielastic neutron scattering and x-ray diffraction experiments

Rémi Busselez,[1] Arantxa Arbe,[2,a)] Fernando Alvarez,[2] Juan Colmenero,[3] and Bernhard Frick[4]

[1]*Donostia International Physics Center, Paseo Manuel de Lardizabal 4, E-20018 San Sebastián, Spain*
[2]*Centro de Física de Materiales (CSIC, UPV/EHU) and Materials Physics Center MPC, Paseo Manuel de Lardizabal 5, E-20018 San Sebastián, Spain*
[3]*Donostia International Physics Center, Paseo Manuel de Lardizabal 4, E-20018 San Sebastián, Spain, Centro de Física de Materiales (CSIC, UPV/EHU) and Materials Physics Center MPC, Paseo Manuel de Lardizabal 5, E-20018 San Sebastián, Spain*
[4]*Institut Laue Langevin, BP 156, 38042 Grenoble Cedex 9, France*

(Received 6 September 2010; accepted 14 December 2010; published online 3 February 2011)

Quasielastic neutron scattering, x-ray diffraction measurements, and fully atomistic molecular dynamics simulations have been performed on poly(vinylpyrrolidone) homopolymer above its glass transition temperature. A "prepeak" appears in the x-ray diffraction pattern that shows the typical features of a first amorphous halo. From an effective description of the experimentally accessed incoherent scattering function of hydrogens in terms of a stretched exponential function, we observe enhanced stretching and a momentum-transfer dependence of the characteristic time different from that usually reported for more simple polymers (main-chain polymers or polymers with small side groups). The comparison with both kinds of experimental results has validated the simulations. The analysis of the simulated structure factor points to a nanosegregation of side groups (SG) and main-chains (MC). The detailed insight provided by the simulations on the atomic trajectories reveals a partial and spatially localized decoupling of MC and SG dynamics at length scales between the average SG–SG distance and the characteristic length of the backbone interchain correlations. Anomalous behavior in correlators calculated for the SG subsystem are found, like e.g., logarithmiclike decays of the density–density correlation function. They might be a consequence of the existing large dynamic asymmetry between SG and MC subsystems. Our results suggest that, as the SGs are spatially extended and chemically different from the backbone, they form transient nanosegregated domains. The dynamics of these domains show similar behavior to that found in other systems displaying large dynamic asymmetry. © *2011 American Institute of Physics*. [doi:10.1063/1.3533771]

I. INTRODUCTION

Addition of side groups in polymers can lead to complex and interesting properties in terms of apparition of secondary relaxations and existence of new correlation lengths.[1–3] Moreover, it has been shown that increasing the size of side groups has a deep impact on the structure and dynamics of polymers. Of particular interest is the family of poly(*n*-alkyl-methacrylates),[2,4–12] where x-ray and neutron diffraction analysis show that nanosegregation occurs between backbone and side groups. The effects of these nanosegregated domains on the local dynamics remain however unclear. In particular, the hypothetic presence of two types of α relaxation is discussed in poly(*n*-alkyl-methacrylates) and poly(di-*n*-alkyl itaconates).[12–14] Two structural relaxations have also been reported for poly(isobornyl methacrylate), a polymer with a bulky bicyclic isobornyl side group.[15] In order to clarify the role played by side groups dynamics, it can be useful to reduce the complexity herited from them. This can be achieved by reducing the intrinsic degrees of freedom of side groups, i.e., taking a rigid side group. One of the polymers owning these characteristics is poly(vinylpyrrolidone) (PVP). As the pyrrolidone side groups consist of a nitrogen with four membered carbon ring attached to a vinylic backbone (see inset in Fig. 1), we can expect a huge steric hindrance from the pyrrolidone ring.

Here we present a study of PVP by x-ray diffraction, quasielastic neutron scattering (QENS), and fully atomistic molecular dynamics (MD) simulations. The spatial and dynamic ranges explored by these techniques (i.e., typically covering the angstrom length scale and nanosecond time scale) are adequate for studying the short-range order and the molecular motions involved in the structural relaxation of this polymer. Our experiments have revealed features that are not found in main-chain polymers or in polymers with small side groups, like a "prepeak" in the diffraction pattern and unusual stretching of the incoherent scattering function for hydrogen motions. These peculiar properties are also displayed by the simulated cell. MD simulations offer information of

a)Electronic mail: a.arbe@ehu.es.

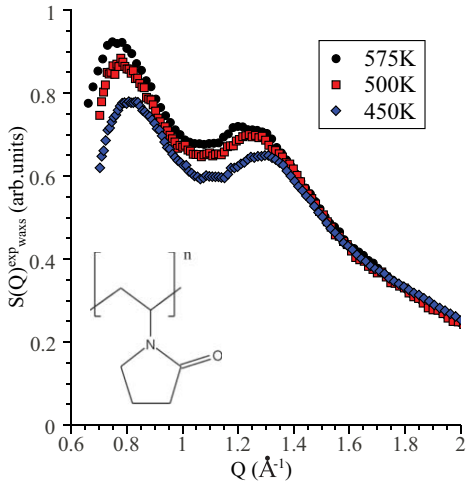

FIG. 1. X-ray diffraction patterns of PVP measured at different temperatures. The chemical formula of PVP is shown in the inset.

utmost interest for the interpretation of these results, that cannot be accessed by the experiments. For example, they allow real space analysis, easy discrimination of different atomic species, and coarse-graining methods. Therefore, our strategy has been the following. We have first validated the structure of the simulated cell by direct comparison of the x-ray diffraction data with the simulated counterparts (Sec. III A). For validating the dynamics, we have analyzed the QENS results and the analogous computed functions in the same way and compared the respective results (Sec. III B). Then, we have exploited the simulations to gain insight in the details of the local structure and dynamics (Sec. IV). To do this, we have first considered an atomistic approach (Sec. IV A) where the total structure factor including all atoms in the system and the motions of the hydrogen atoms have been studied. We note that this can be considered as an "experimental" approach, since the functions investigated are those potentially accessible by neutron scattering experiments (diffraction on fully deuterated samples and QENS on protonated samples, respectively). The analysis of the contributions of the different molecular groups (main chain, MC and side groups, SG) to the static structure factor suggest nanosegregation. Strong dynamic heterogeneity is found for the different kinds of hydrogens. We also find an additional non-Gaussian regime in the self-motions with respect to chemically simple polymers that occurs at intermediate length scales between the SG/SG and the MC/MC average distances. Thereafter, we have coarse-grained the system considering the centers of mass of the pyrrolidone ring and the vinyl group and eliminating thereby nonessential ingredients (Sec. IV B). The main peculiarities observed for hydrogen atoms persist in the coarse-grained system, confirming their genuine nature. The structural relaxation of MCs takes place at much longer times than that of the SGs (large dynamic asymmetry), and the latter shows anomalous behavior manifested, e.g., by logarithmiclike decays. We speculate that nanosegregation could be at the origin of these anomalous dynamical properties. Finally, scenario for PVP is discussed.

II. METHODS

A. Sample

PVP in aqueous solution (55 wt.%) was purchased from Aldrich Chemical and was used without any further purification. The reported weight—average molecular weight (M_w) of this polymer is 160 Kg. mol^{-1}. The dry sample was obtained by evaporating water from the initial solution in a vacuum oven at 400 K during a week. The sample studied by x-ray diffraction was a film of 0.75 mm thickness, while that investigated by QENS was prepared directly in an aluminium flat holder in which thickness was chosen to insure more than 90% of transmission (0.2 mm). The glass transition temperature T_g of the sample was determined by a differential scanning calorimetry (DSC) scan to be 445 K in agreement with existing dynamic mechanical analysis and DSC studies on this homopolymer.[16,17]

B. X-ray diffraction

Diffraction experiments were performed using a Rigaku SAXS apparatus with WAXS image plate chamber. The MicroMax-002+ x-ray generator system is comprised of a microfocus sealed tube x-ray source module and an integrated x-ray generator unit. Using $Cu\ K_\alpha$ transition photons of wavelength $\lambda = 1.5418$ Å are provided. As image plates are used for WAXS detection, a conversion of the intensity measured in absolute units is not easy and the results are delivered in arbitrary units. With a Linkam temperature control insuring a temperature stability of ± 0.5 K we investigated the sample at 450, 500, 550, and 575 K.

C. Quasielastic neutron scattering

In a QENS neutron scattering experiment, the measured intensity as a function of energy $\hbar\omega$ and momentum transfer $\vec{Q}$ provides information on the dynamics and structure of the sample under investigation. The modulus of the momentum transfer Q is determined by the scattering angle θ and the wavelength of the incoming neutrons λ as $Q = 4\pi \sin(\theta/2)/\lambda$. The measured intensity contains incoherent and coherent contributions that are weighted according to the isotope depending cross sections ($\sigma^\alpha_{\rm inc}$, $\sigma^\alpha_{\rm coh}$) where α refers to the isotope considered. The incoherent scattering function of isotope α $S^\alpha_{\rm inc}(Q,\omega)$ is the time Fourier transform of the intermediate incoherent scattering function $F^\alpha_s(Q,t)$ and the time and space Fourier transforms of $S^\alpha_{\rm inc}(Q,\omega)$ yield the self part of the Van Hove correlation function $G^\alpha_s(r,t)$

$$G^\alpha_s(r,t) = \frac{1}{N_\alpha}\left\langle \sum_{i=1}^{N_\alpha} \delta\left[|\vec{r} - \left(\vec{r}^\alpha_i(t) - \vec{r}^\alpha_i(0)\right)|\right]\right\rangle, \qquad (1)$$

where N_α is the number of nuclei of the considered kind of isotope α in the sample. In the classical limit, $G^\alpha_s(r,t)$ is the probability of a given nucleus α to be at distance r from the position where it was located at a time t before ($\vec{r}^\alpha_i$ denotes the position of the particle i and the brackets mean thermal average). Incoherent scattering is determined by correlations between the positions of the same nucleus at

different times. On the other hand, coherent scattering gives information about the relative positions of two nuclei (see, as a general reference, Ref. 18). The incoherent cross-section of hydrogen is much larger than any other cross section of the atoms constituting PVP. Therefore, we assume that the coherent scattering contribution is negligible and thus the measured signal $S^{\text{exp}}(Q,\omega)$ is dominated by the scattering from hydrogens, providing thus information about the self-motion of such atoms through $S^{H}_{\text{inc}}(Q,\omega)$.

1. Backscattering measurements

We measured $S^{\text{exp}}(Q,\omega) \approx S^{H}_{\text{inc}}(Q,\omega)$ in PVP at two temperatures, 550 and 575 K, by the backscattering instrument IN16 (Ref. 19) at the Institute Laue-Langevin (ILL) in Grenoble. With a wavelength of 6.271 Å an energy resolution (full width at half maximum) of 0.9 μeV with a nearly Gaussian shape is achieved and a Q range from 0.2 to 1.9 Å^{-1} is covered. The resolution function of the spectrometer $R(Q,\omega)$ was determined from the measurement of the sample at 2 K, where the scattering is considered elastic in this experimental window. The acquired data were corrected for detector efficiency, sample container, and absorption using the standard programs available at ILL.

D. Molecular dynamics simulations

The simulations were carried out using materials studio 4.1 and the DISCOVER-3 module from ACCELRYS with the COMPASS force field.[20,21] Most parameters of this force field are derived from *ab initio* calculations and later optimized empirically to yield good agreement with experiments. As for many force fields, the functional form is divided in two different contributions, namely bonded and nonbonded terms. Bonded terms are representing different intramolecular potentials namely bonding, angular, torsional, and out of plane potentials described as sums of quartic terms. Nonbonded terms are grouping Coulombic and Van der Waals potentials. It has to be noted that Van der Waals potentials are described as a 6-9 Lennard-Jones potential form rather than the commonly used 6-12 Lennard-Jones potential. The infinite sum of Coulombic terms has been truncated using a group-based spherical cutoff method with a cutoff radius $R_c = 12$ Å. The potential obtained is thereafter multiplied with a switching function in order to slowly decrease the potential to zero yielding to a continuous potential energy and derivates. We used a switching function of 1 Å of extension, value that is encountered to give correct results for a number of polymers.[22–24]

The simulated system was built using the amorphous cell protocol[25,26] implemented in Material Studio. A cubic cell containing six polymers chains of 100 monomers units of vinyl pyrrolidone was constructed under periodic boundary conditions. After the creation of such a cell, standard minimization protocols have been used in order to minimize the energy structure via a Polak–Ribiere algorithm. Then from this point the system was equilibrated at 700 K for 5 ns using NPT canonical ensemble (i.e., keeping the numbers of atoms (N), the pressure (P), and temperature (T) constant). Afterwards, the resulting cell has been equilibrated at 575 K during 20 ns in another NPT canonical ensemble. Accumulation of coordinates has been realized following the same procedure at each temperature: first, a primary equilibration of the system size has been reached in an NPT system during 5 ns; after that, we performed a short acquisition simulation of 1 ns in an NVT canonical ensemble (i.e., keeping the numbers of atoms (N), the volume (V), and temperature (T) constant) recording the coordinates every 0.01 ps. Then a longer simulation using the same parameters and ensemble was performed. In this case coordinates were recorded every 0.5 ps. Size of simulation cell and the corresponding densitiy for each temperature studied are shown in Table I.

TABLE I. Size and density of the simulation cell for the temperatures investigated.

Temperature (K)	650	575	550
Size (Å)	48.397	48.301	48.244
Density (g cm^{-3})	0.967	0.977	0.976

1. Computed magnitudes

From the atomic trajectories obtained in the simulations, we have calculated different physical parameters. As this work is mainly dealing with neutron scattering experiments on protonated samples, one of the most fundamental functions is $G^{H}_{s}(r,t)$ (Ref. 27) [Eq. (1)].

We can also define different parameters namely the mean squared displacement, the second moment of $G^{\alpha}_{s}(r,t)$

$$\left\langle r^2_{\alpha}(t)\right\rangle = \int_0^{+\infty} 4\pi r^4 G^{\alpha}_{s}(r,t)\,dr. \tag{2}$$

In the simplest case, $G^{\alpha}_{s}(r,t)$ can be approximated by a Gaussian function

$$G^{\alpha}_{s}(r,t) = \left(\frac{3}{2\pi\left\langle r^2_{\alpha}(t)\right\rangle}\right)^{\frac{3}{2}} \exp\left(-\frac{3r^2}{2\left\langle r^2_{\alpha}(t)\right\rangle}\right). \tag{3}$$

This approximation is valid in numerous cases, as harmonic vibrations in crystals, diffusion of particles in a gas, simple diffusion in liquids, and more generally for systems where motions are governed by Langevin equations.[28] However, in complex systems deviations from this Gaussian form can be found. These deviations can be quantified by the non-Gaussian parameter $\alpha_2(t)$ defined from the cumulants of fourth and second order of $G^{\alpha}_{s}(r,t)$

$$\alpha_2(t) = \frac{3}{5}\frac{\left\langle r^4_{\alpha}(t)\right\rangle}{\left\langle r^2_{\alpha}(t)\right\rangle^2} - 1. \tag{4}$$

In the case of Gaussian $G^{\alpha}_{s}(r,t)$, $F^{\alpha}_{s}(Q,t)$ is also Gaussian and according to Eq. (3) can be written as

$$F^{\alpha}_{s}(Q,t) = \exp\left(-\frac{Q^2\left\langle r^2_{\alpha}(t)\right\rangle}{6}\right). \tag{5}$$

It has to be noted that $G^{\alpha}_{s}(r,t)$, its moments, and subsequently $\alpha_2(t)$ cannot directly be accessed experimentally.

On the other hand, the short-range order of the polymer is characterized by the total static structure factor

$$S(Q) = \langle \rho(\vec{Q})\rho^*(\vec{Q})\rangle \tag{6}$$

with the density operator

$$\rho(\vec{Q}) = \sum_i \exp(-\imath\, \vec{Q}\vec{r}_i), \tag{7}$$

where all atoms are considered. The total structure factor can also be decomposed in partial structure factors, where only atoms belonging to given species are included. Experimentally the structural information is accessed by diffraction methods where the contributions to the structure factor are affected by the atomic scattering form factors $f_\alpha(Q)$ in the following way

$$\rho(\vec{Q}) = \sum_i f_\alpha(Q)\exp(-\imath\, \vec{Q}\vec{r}_i^{\,\alpha}). \tag{8}$$

In the case of neutron scattering, $f_\alpha(Q)$ is independent of the Q value and is hence a constant that only depends on the isotope considered. However, for x rays the atomic scattering length does not only depend on the nature of the atom but also on the Q value. In order to evaluate x-ray atomic structure factors, we refer to the tabulated values found in Ref. 29, expressing the Q-dependent atomic scattering length in terms of a sum of three exponentials plus a constant.

Finally, the coherent intermediate scattering function for α species $F^\alpha_{\rm coh}(Q,t)$ can be calculated as

$$F^\alpha_{\rm coh}(Q,t) = \langle \rho_\alpha(\vec{Q},t)\rho^*_\alpha(\vec{Q},0)\rangle, \tag{9}$$

from the time-dependent density correlator for α species

$$\rho_\alpha(\vec{Q},t) = \sum_j \exp\left(-\imath\, \vec{Q}\vec{r}^{\,\alpha}_j(t)\right). \tag{10}$$

III. EXPERIMENTAL RESULTS AND VALIDATION OF THE SIMULATION

A. Structure

The x-ray diffraction patterns measured on PVP at different temperatures are plotted in Fig. 1. Below $Q \approx 2$ Å^{-1} they show two distinct peaks. One peak appears around 1.2 Å^{-1}, i.e., in the region where usually amorphous "simple" polymers [main-chain polymers like e.g., polybutadiene[30] or polymers with small side groups like e.g., poly(ethylene propylene)][31] show their first or "main" structure factor peak, also called amorphous halo. At lower Qs, around 0.7 Å^{-1}, a "prepeak" is present. The intensity of the prepeak is higher than that of the main diffraction peak. With increasing temperature, the intensity increases and the position shifts toward lower Q values for both peaks. This is the usual behavior shown by the "main" peak in simple polymers. The shift is generally attributed to an expansion of the system leading to larger interchain average distances. The observed effects are more pronounced in the temperature interval 400–500 K than between 500 and 575 K, and the influence on the intensity is larger for the peak at ≈0.7 Å^{-1}.

In Fig. 2 the x-ray structure factors calculated from the MD simulations at the different temperatures investigated are plotted together with that measured at 550 K. A reasonable agreement is found between the results from both techniques at the same temperature. Moreover, the simulated patterns show a similar T-dependence to that observed experimentally (Fig. 1). From this comparison we conclude that our simulations reproduce sufficiently well the local structure.

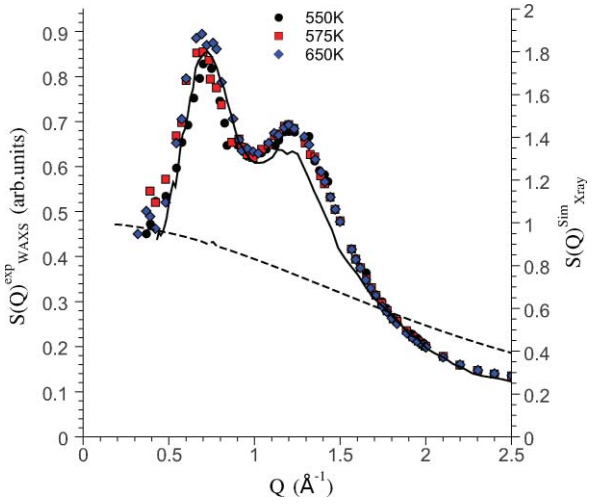

FIG. 2. X-ray diffraction pattern of PVP measured at 550 K (black solid line) and obtained from simulations at different temperatures (symbols). Dashed line: Form factor obtained from simulations.

B. Dynamics

1. QENS results

As mentioned above, the intensity scattered from fully hydrogenated molecules like those in our sample essentially corresponds to the incoherent scattering function of protons $S^H_{\rm inc}(Q,\omega)$. In particular, due to the morphology of PVP (see Fig. 1), where six over nine hydrogens belong to the pyrrolidone ring, the largest contribution is that of the self-correlation of the hydrogens of the side groups.

The temperatures measured, 550 and 575 K, are well above T_g. As can be seen in Fig. 3, in this temperature range $S^{\rm exp}(Q,\omega)$ appears essentially as a quasielastic line. The absence of elastic contributions indicates a diffusivelike motion. For glass-forming polymers well above T_g, it is usually found that $F^H_s(Q,t)$ decays in two steps. The first fast decay takes place at times below ≈2 ps and the second slow decay has a characteristic time that strongly depends on temperature and also varies with Q.[32] In the energy-transfer window accessed by backscattering techniques, the scattering function is mainly determined by the features of the slow decay of $F^H_s(Q,t)$ that can usually be described by a Kohlrausch–Williams–Watts (KWW) functional form

$$F^H_s(Q,t) = A(Q)\exp\left[-\left(\frac{t}{\tau_{\rm KWW}(Q)}\right)^{\beta(Q)}\right]. \tag{11}$$

This stretched exponential law is a convenient empirical way to reproduce relaxation functions of glass-forming materials above $t \approx 2$ ps. Here, $\tau_{\rm KWW}$ stands for the characteristic relaxation time, whereas β reflects the non-Debye character of

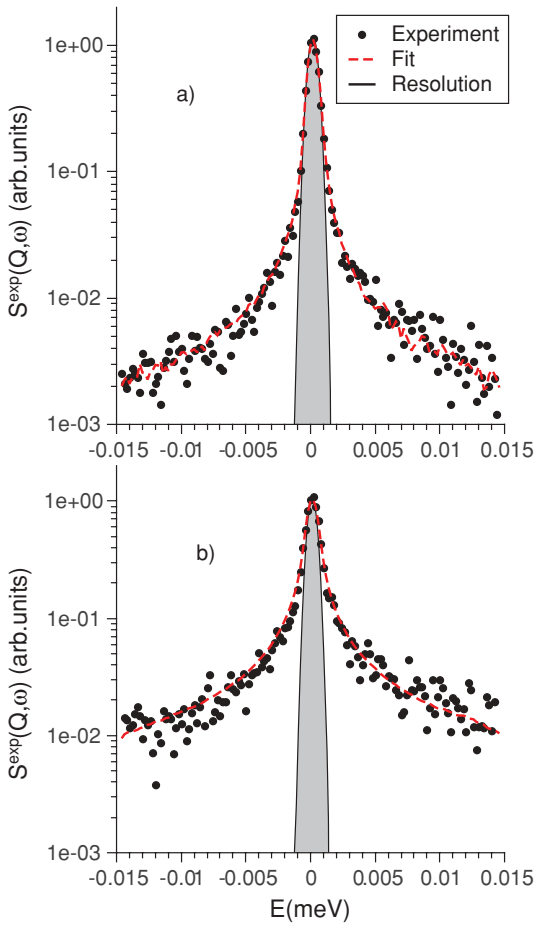

FIG. 3. Quasielastic neutron scattering spectra at 575 K for two Q values: 0.54 Å^{-1} (a) and 1.49 Å^{-1} (b). In the KWW fits [Eq. (13)] β was 0.35.

the relaxation function. It usually takes values close to 0.5 for regular polymers.[33] The contribution of the fast modes (vibrations, librations, etc. leading to the fast decay before ≈2 ps) is parametrized as an overall intensity loss expressed by $A(Q)$ which is usually approximated by a Lamb–Mössbauer-like factor

$$A(Q) = \exp\left(-\frac{\langle u^2\rangle Q^2}{3}\right), \tag{12}$$

with $\langle u^2\rangle$ the vibrational mean squared displacement.

This kind of description is expected to hold for PVP main-chain hydrogens. In principle, the dynamics of SG hydrogens can be more complex and may include additional local reorientational motions. At high enough temperature, however, the total relaxation function is usually dominated by the diffusivelike process[34,35] and can be approximated by Eq. (11), though a different β value could be expected due to the underlying superposition of motions. Thus, both MC and SG contributions to the measured scattering function would be describable by Eq. (11), with in principle different values for the involved parameters. Unfortunately, from the experimental data it is impossible to univocally determine values of all these parameters. Therefore, we have used a unique KWW function to effectively describe the overall H-dynamics in our system. We note that the versatile KWW functional form can describe an intrinsically stretched relaxation function and also a superposition of relaxation processes.[36]

The experimental data have thus been fitted at each Q value by the Fourier transform of Eq. (11) convoluted with the experimental resolution

$$S^{\rm exp}(Q,\omega) = R(Q,\omega) \otimes \times \int_0^{+\infty} \exp(-\imath\omega t)\, A(Q) \exp\left[-\left(\frac{t}{\tau_{\rm KWW}(Q)}\right)^{\beta(Q)}\right] dt. \tag{13}$$

In a first approach, we fitted the data letting all the parameters free [$\tau_{KWW}(Q)$, $\beta(Q)$ and $A(Q)$]. No significant and systematic Q dependence could be determined for β, which average value was $\langle\beta^{\rm exp}\rangle = 0.35$. This value is notably smaller than that usually found for regular polymers, as expected. However, *a priori* one cannot determine the origin of this enhanced stretching. It could be due to a more complex dynamics of SG hydrogens, to heterogeneity in the dynamics of MC and SG atoms, or to both. Fixing $\beta = \langle\beta^{\rm exp}\rangle = 0.35$ in the fits the amplitude and relaxation times of the KWW functions were refined. This procedure provides good fits of the data as shown by the dotted lines in Fig. 3.

The fits give the dispersion curve of relaxation times displayed in Fig. 4. We can see a monotonic variation of the logarithm of the relaxation time $\tau_{\rm KWW}(Q)$ with respect to the logarithm of Q, following an approximative $\tau_{\rm KWW}(Q) \propto Q^{-3}$ power law. This behavior is not commonly encountered in the field of polymer dynamics. Previous works on polymers (see for instance[23,37,38]) and glass formers[39,40] have reported a crossover in the Q dependence of the relaxation

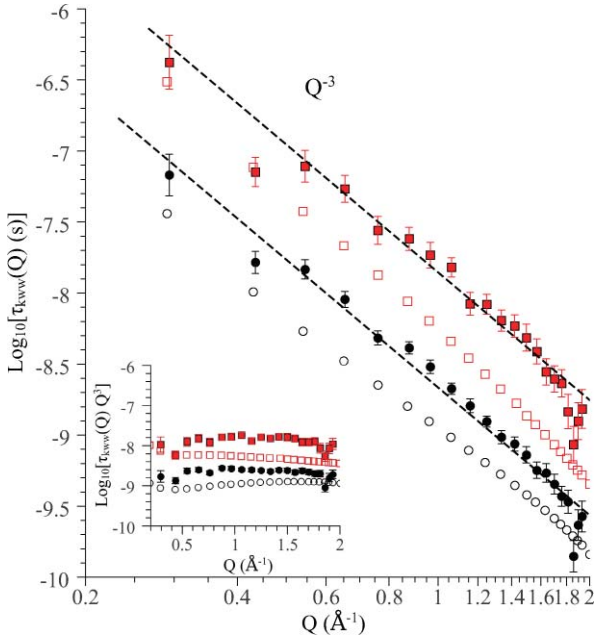

FIG. 4. Q dependence of the logarithm of the relaxation times of $F_s^H(Q,t)$ as observed by QENS (solid symbols) and calculated from the simulations (empty symbols) at 550 (squares) and 575 K (circles). A Q^{-3} behavior of the times is visible. Accordingly, the inset shows that the times multiplied by Q^3 hardly depend on Q.

times taking place around a Q-value Q_c^* which usually corresponds to the intermolecular position characterized by the main diffraction peak $Q_{\max}$. In those cases, the exponent x of the Q^{-x} dependence of $\tau_{\mathrm{KWW}}(Q)$ changes from $x \simeq 2$ at $Q \gtrsim Q_c^*$, to $x = 2/\beta$ indicative for Gaussian behavior at lower Q.[41]

2. Simulation results

To validate the simulations from a dynamic point of view we have calculated $F_s^H(Q,t)$ from the trajectories and analyzed its decay in an analogous way, i.e., by means of a KWW model [Eq. (11)]. Some examples of the calculated correlators at 575 K and their corresponding fits are shown in Fig. 5. The stretched exponentials describe well the slow decays of the scattering functions. In particular, in the equivalent time-range covered by IN16 (≈0.2...4 ns) the description is excellent. The β parameters used are between 0.2 and 0.5 in the range considered [see later in Fig. 8(b)]. We note that the average value extracted from our simulations for the Q range covered by IN16 (around 0.4) is close to $\langle\beta^{\mathrm{exp}}\rangle = 0.35$. The resulting characteristic times for 550 and 575 K are compared with those from IN16 in Fig. 4. The Q dependences of experimental and simulated dispersion curves are in very good agreement, though the absolute values of $\tau_{\mathrm{KWW}}(Q)$ differ by a factor 2 constant in Q and temperature. We note that shifts in temperature and/or timescale are usually required for a perfect matching of results from MD simulations and real samples. We can mention the cases of orthoterphenyl,[42] polyisoprene,[43] poly(methyl methacrylate),[5,44] poly(vinyl acetate),[45] poly(ethylene propylene),[31] and poly(vinyl methyl ether).[46] Apart from slight differences in the microstructure or in the density, a possible source for this discrepancy could be that the force field used in the simulations was not perfectly calibrated. For the case of polybutadiene, Smith *et al.*[47] showed that the time scale of the α relaxation resulting from the MD simulations is quite sensitive to slight changes in the local intrachain potentials. Regarding the values of the mean squared displacements due to vibrations obtained from the amplitudes of the KWW functions, we find a reasonable agreement between experiments and simulations: at 550 K, $\langle u^2_{\mathrm{exp}}\rangle = 0.98$ Å^2 and $\langle u^2_{\mathrm{exp}}\rangle = 1.03$ Å^2 and at 575 K, $\langle u^2_{\mathrm{exp}}\rangle = 1.00$ Å^2, and $\langle u^2_{\mathrm{exp}}\rangle = 1.18$ Å^2. Thus, besides the small shift in the timescale, we observe a very good coincidence of experimental and simulated results, indicating that the simulated cell provides a good mimic of the real polymer also from a dynamical point of view (at least at the time and spatial scales here investigated).[48]

IV. EXPLOITING THE SIMULATIONS

Once the reliability of the simulations has been proved, we can get deeper insight in both, the structural and dynamical features of PVP, exploiting the capabilities of the simulations.

A. Atomistic approach

1. Short-range order in PVP

The x-ray structure factor is affected by the corresponding atomic scattering form factors [Eqs. (6) and (8)] and to discuss the structural features of the sample it is more convenient to calculate the total structure factor (Eqs. (6) and (7), i.e., $f^{\alpha}(Q) = 1$ for all α and Q values).[49] The results at 650 K are displayed in Fig. 6 (black circles). They show the same main features as the x-ray diffraction patterns (both peaks at $Q \approx 0.6$ and 1.2 Å^{-1}), though with different relative amplitude. As the total structure factor contains all the

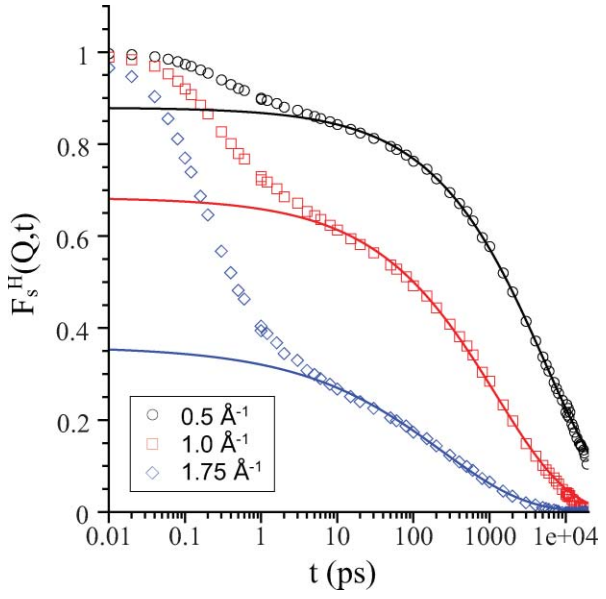

FIG. 5. $F_s^H(Q,t)$ obtained from the simulations at 575 K for three different Q values. Solid lines are KWW fits of the decay at $t \gtrsim 10$ ps in order to avoid the contribution of the first fast decay. The shadowed area shows the equivalent time-window covered by IN16.

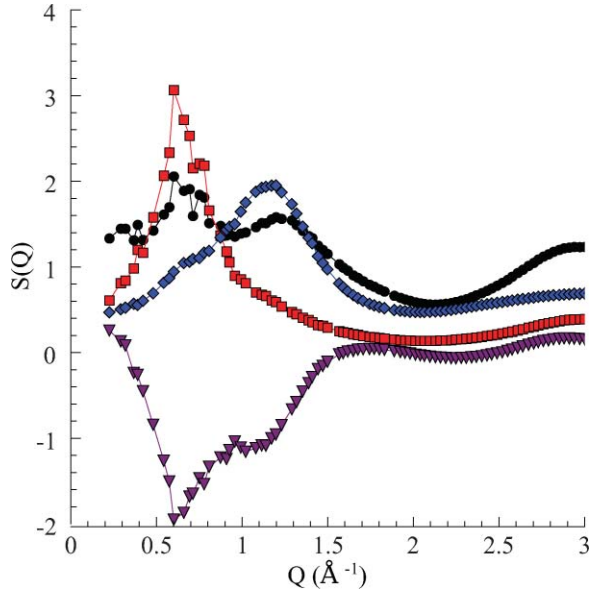

FIG. 6. Structure factor (black circles) of PVP obtained from the simulations at 650 K. The partial contributions due to MC/MC chain correlations (red squares), SG/SG correlations (blue diamonds) and cross-correlations between MC and SG (purple triangles) are displayed.

pair correlations in the system, it becomes difficult to extract a detailed view of the short-range order only from this observable. Therefore, we have regrouped different atoms according to their relative position in the monomer, either in the main chain or in the side group and decomposed the total structure factor into the partial structure factors of the MC atoms, $S_{MC/MC}(Q)$, the SG atoms, $S_{SG/SG}(Q)$, and the cross-correlations $S_{MC/SG}(Q)$ (see Fig. 6). $S_{MC/MC}(Q)$ shows a strongly marked peak around 0.6 Å^{-1}. This peak is roughly in the same position as the "prepeak" in the x-ray pattern, reinforcing the idea that in polymers with bulky side groups such a "prepeak" is representative of the polymer backbone distance.[11,12,14,50,51] This average distance could be estimated from the peak position as $2\pi/0.6$ Å^{-1} = 10.5 Å. $S_{MC/MC}(Q)$ smoothly decreases toward higher Q but still shows a small shoulder around 1.2 Å^{-1}, i.e., around the "main" peak. Looking now at the correlations between side groups $S_{SG/SG}(Q)$, we can see a broad peak around 1.3 Å^{-1} with a slight shoulder around 0.6 Å^{-1}. Thus, in PVP the "main" peak around 1.2Å^{-1} is mainly due to correlations involving side groups. The cross-correlations between MC and SG atoms $S_{MC/SG}(Q)$ are negative and very pronounced in the Q range from 0.4 to 1.4 Å^{-1}. Where the correlations among atoms belonging to the same subgroups are strongly marked, the cross-correlations between subgroups are negative and approximately mirror both main peaks. In definitive, for $Q \lesssim 2$ Å^{-1}, the simulated structure shows two clearly separated peaks, each of them mainly corresponding to strong correlations among atoms belonging to either MCs or SGs. Strong negative cross-correlations also contribute to them to a large extent. These features are characteristic of a local separation between the distinct components of the polymer (MC and SG). Similar features, that have been attributed to reflect a precursor effect of nanosegregated phases have been reported for polymers with relatively large side groups like poly(methyl methacrylate) or poly(vinyl acetate).[45] In such systems, structural segregations can be relatively important and also affect the dynamics of the system. An extreme case can be found in the family of poly(*n*-alkyl-methacrylates), poly-(alkyl-acrylates), and poly-(*n*-itaconates) where nanophase segregation is well developed and has a strong impact on the dynamics.[4–6,10,11,50–54]

2. Intrinsic heterogeneities in the H-dynamics

a. Reciprocal space analysis. The different kinds of hydrogens (those in the main chain, H_{MC}, and those in the side group, H_{SG}) can easily be discriminated from the simulations. We have thus calculated separately the corresponding intermediate incoherent scattering functions, $F_s^{H_{MC}}(Q,t)$ and $F_s^{H_{SG}}(Q,t)$. As an example, Fig. 7 shows the results for 550 K and $Q = 0.87$ Å^{-1}. At these conditions, the second decay is more stretched for $F_s^{H_{SG}}(Q,t)$ than for $F_s^{H_{MC}}(Q,t)$, as deduced from the smaller β value of the KWW fit. We note that, as in Fig. 5, this effective KWW description is also good for the slow decay of $F_s^{H}(Q,t)$. As the contributions of $F_s^{H}(Q,t)$ are ponderated by the relative number of hydrogens belonging to each group, the parameters characterizing the behavior of the hydrogens of the entire system are closer to those of H_{SG}. The different parameters extracted from the KWW analysis at 575 K are shown in Fig. 8. The amplitude [Fig. 8 (a)] is larger for H_{MC} than for H_{SG}, and this difference is enhanced with increasing Q. This indicates that the fast motions of H_{MC} are much more localized than those of H_{SG}. The amplitudes follow well a Lamb–Mössbauer-like factor expression [Eq. (12)] only at small Q values. Fits to Eq. (12) in the range $Q^2 \lesssim 3$ Å^{-2} deliver the values $\langle u^2_{H_{MC}}\rangle = 0.66$ Å^2, $\langle u^2_{H_{SG}}\rangle = 1.49$ Å^2. The clearly smaller amplitude of H_{MC} relates to librational degrees of freedom which are not available for the main chain, while the stronger decay indicates larger mobility of the side groups in the microscopic regime. The flattening of the amplitudes at larger Q values indicates relatively strong deviations from Gaussian approximation of the dynamics in the fast regime. The stretching exponent β [Fig. 8(b)] strongly decreases with increasing Q, roughly coinciding for both subspecies in the low and high Q regions and being smaller for H_{SG} than for H_{MC} at intermediate Q values. We note the extreme stretching at local scales. Focusing on the mean relaxation times $\langle\tau\rangle = \tau_{KWW}\Gamma(1/\beta)/\beta$ [Fig. 8(c)], we observe that for $Q \gtrsim 2$ Å^{-1} they display roughly the same values for H_{MC} and H_{SG} and follow a Q^{-3} law. For $Q \lesssim 2$ Å^{-1} MC and SG mean relaxation times decouple, showing two different Q^{-x} behaviors. For H_{MC}, a single power-law $Q^{-2.5}$ is observed down to the lowest Q value investigated. The relaxation time of H_{SG} follows a Q^{-2} law between 0.6 and 2 Å^{-1}, and a second cross over takes place around $Q \simeq 0.6$ Å^{-1}, where the $\langle\tau\rangle$ behavior changes to $Q^{-3.5}$ at lower Q values. The characteristic times of both populations seem to converge again in the low-Q limit. Thus, as compared to regular polymers, where *one* crossover takes place within the usual backscattering Q range separating a Gaussian from a non-Gaussian regime, PVP hydrogens show a more complex situation. Finally we note that, though the relaxation times of all the hydrogens are mainly determined by the statistically dominant population (i.e., H_{SG}), in the resulting average the crossovers observed for H_{SG} are smeared out

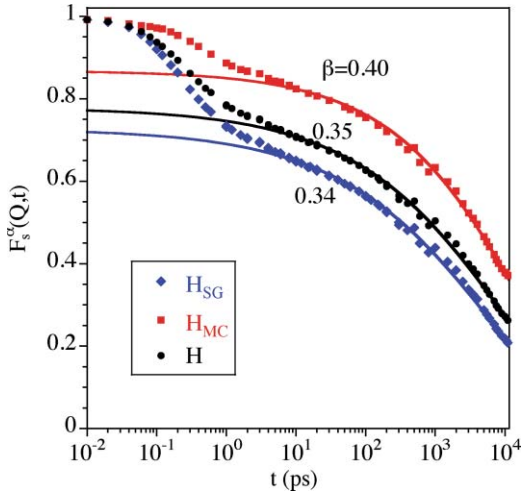

FIG. 7. Intermediate incoherent scattering function obtained from the simulations at 550 K and $Q = 0.87$ Å^{-1} for H_{MC}, H_{SG} and all Hs. Solid lines are KWW fits of the slow decay with the indicated values of the β-parameter.

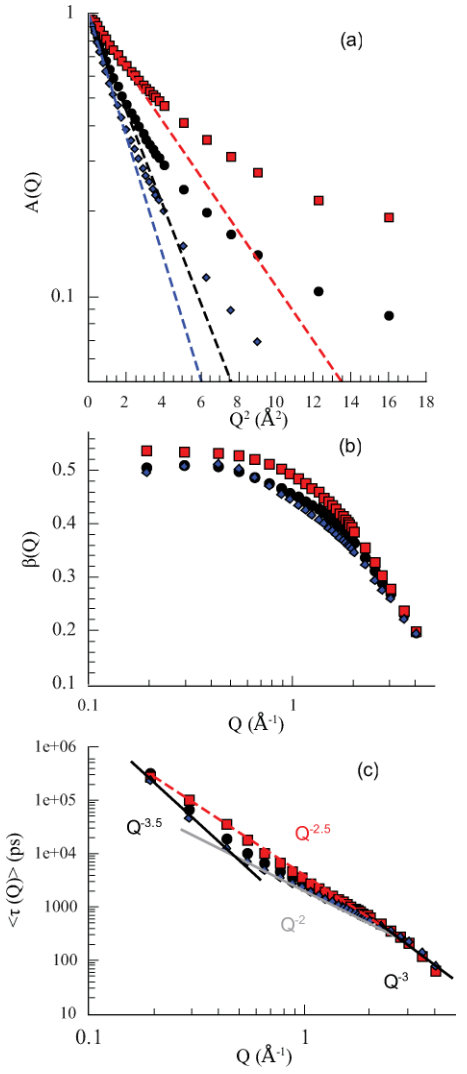

FIG. 8. Q dependence of the KWW parameters obtained from the analysis of the simulated intermediate scattering function at 575 K. (a) Amplitude of the KWW function. (b) Exponent parameter. (c) Mean relaxation time. Black circles: all hydrogens, red squares: main-chain hydrogens, blue diamonds: side-groups hydrogens.

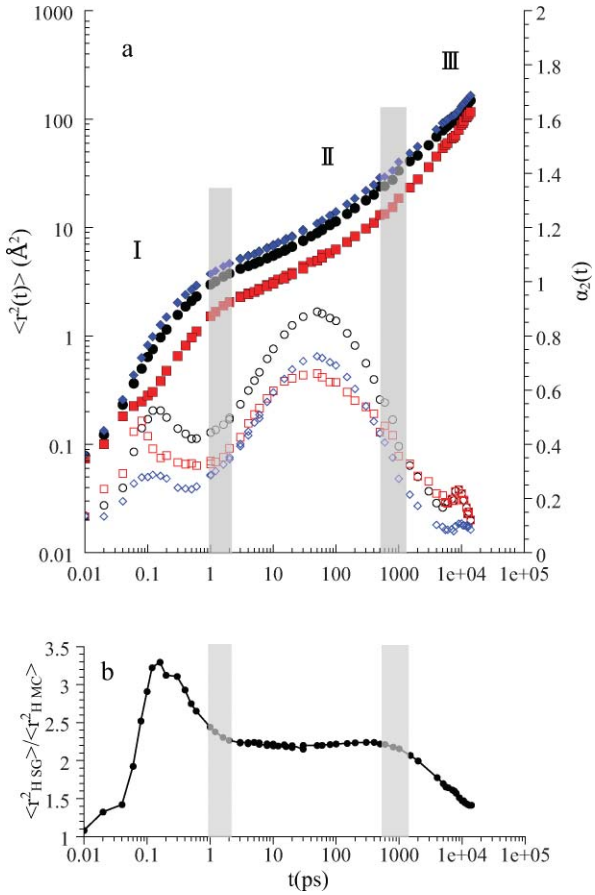

FIG. 9. (a) Mean squared displacement (full symbols) and non-Gaussian parameter (empty symbols) of all hydrogens (black circles), of H_{MC} (red squares) and H_{SG} (blue diamonds). (b) Ratio between the mean squared displacements of the side-group hydrogens and the main-chain hydrogens as function of time. All calculations were done at 650 K. Shadowed regions show the transitions between the three regimes distinguished.

and an effective continuous Q^{-3} description applies, which is close to that experimentally found. Thus, the simulations resolve fine features of the dynamics that are hidden in the experiments.

b. Real space analysis. Figure 9 shows the mean squared displacement and the non-Gaussian parameter of the hydrogen atoms [$\langle r_H^2(t)\rangle$ and $\alpha_2^H(t)$] at 650 K. Here we have also discriminated the contributions of the two subgroups (H_{MC} and H_{SG}). The parameters relative to the different subgroups are not equivalent. The resulting $\langle r_H^2(t)\rangle$ resembles that of the side-group hydrogens $\langle r_{H_{\mathrm{SG}}}^2(t)\rangle$, while the total $\alpha_2^H(t)$ is always larger than those of the subgroups. Except for the shortest times, $\langle r_{H_{\mathrm{SG}}}^2(t)\rangle$ are larger than $\langle r_{H_{\mathrm{MC}}}^2(t)\rangle$ in the time range explored by the simulations, as can be seen in their ratio represented in Fig. 9(b). We may distinguish three different time regimes. In the "fast" regime I before ≈1 ps a large difference stands in the vibrational dynamics of both subpopulations. $\langle r_{H_{\mathrm{SG}}}^2(t)\rangle$ grows much more rapidly than $\langle r_{H_{\mathrm{MC}}}^2(t)\rangle$ and a first peak appears in the non-Gaussian parameters reflecting deviations from Gaussian behavior of the vibrational motions, that are more marked for H_{MC}. Regime II, between ≈1 ps and 500 ps...1 ns, corresponds to the "plateaulike" and "decaging" regime. At the beginning of this regime, we observe a tendency toward a plateaulike behavior in the displacements. This plateau corresponds in glass forming systems to the caging regime, where atoms are trapped by their direct neighbors and are rattling inside the traps. In regime II, the non-Gaussian parameters increase and reach a maximum at around 40 ps (for 650 K considered in the figure) that is usually identified with the onset of the decaging process (or the beginning of α relaxation). In the whole regime II over 3 decades the ratio $\langle r_{H_{SG}}^2(t)\rangle/\langle r_{H_{MC}}^2(t)\rangle$ is strikingly constant and around 2.5. At longer times, in regime III, this ratio starts to slowly decrease, indicating that the MC hydrogens display an enhanced mobility and the atomic displacements of both subspecies tend to be indistinguishable. The values of the non-Gaussian parameters are rather small and subdiffusive motions start to take place. This regime can be considered as the crossover region toward Rouse-like dynamics, where microscopic details of the monomer do not play an important

role anymore, the correlation functions are Gaussian and $\langle r^2(t)\rangle \propto t^{0.5}$.

B. Coarse-graining the system

The all-atoms approach presented in the preceding subsection is of special interest due to the possible direct comparison with experimental data. However, focusing on the particular dynamics associated to each kind of the protons can lead to a complex interpretation of the simulated data. In order to probe elementary properties in the polymer, it is possible to perform a coarse-grained analysis of the obtained configurations. Such analysis can be performed by calculating the same correlators on the center of mass (CoM) of each pyrrolidone ring and of each vinyl group. By this way, reducing the number of coordinates, we also decrease the degrees of freedom involved and consequently the number of characteristic lengths and time scales involved, accessing thereby the basic events of such a complex system. For example, the simplified structure can be more easily interpreted e.g., in terms of its inter- and intramolecular contributions. For the sake of simplicity, in this chapter we will denote with the label "MC" the correlations calculated on the CoM of the vinyl groups and with the label "SG" those on the CoM of the pyrrolidone ring.

1. Structure

For 650 K, Fig. 10 displays the coarse-grained partial static structure factors corresponding to MC/MC correlations $S^{\mathrm{CoM}}_{\mathrm{MC/MC}}(Q)$ and SG/SG correlations $S^{\mathrm{CoM}}_{\mathrm{SG/SG}}(Q)$ and their intra- and interchain contributions. Later in Fig. 12(b) we can also see these functions together with the cross-correlation term $S^{\mathrm{CoM}}_{\mathrm{MC/SG}}(Q)$. Compared to the all-atoms counterpart (Fig. 6), the coarse-grained structure is much more marked, although the positions of the peaks are invariant.

$S^{\mathrm{CoM}}_{\mathrm{SG/SG}}(Q)$ shows the typical form of a simple hard sphere fluid [Fig. 10(b)]. The first main peak located at $Q^{\mathrm{SG}}_{\mathrm{max}} \approx 1.3$ Å^{-1} reveals a characteristic average distance between SG centers of mass $d_{\mathrm{SG}} \approx 2\pi/Q^{SG}_{max} = 5$ Å. In the region of $Q^{\mathrm{SG}}_{\mathrm{max}}$ both intra- and interchain contributions are present and developed.

In the same Q range, $S^{\mathrm{CoM}}_{\mathrm{CM/CM}}(Q)$ displays a clear shoulder [Fig. 10(a)]. A peak in this Q range is generally associated to the first coordination shell. In this region the interchain correlations are extremely small and thus we can assign a purely intrachain origin to the shoulder: the first neighboring vinyl groups are those directly linked along the chain backbone.

As in the all-atom analysis and x-ray diffraction pattern, we see an important peak around $Q^{\mathrm{MC}}_{\mathrm{max}} \approx 0.6$ Å^{-1} in the MC structure. Strongly marked contributions from the interchain correlations at this Q value suggest an interchain origin of the "prepeak" (note that intrachain correlations in this Q range are dominated by the polymer form factor and do not display a marked structure). No large-scale correlations contributing to the prepeak can be observed between the ring groups in the coarse-grained analysis. The shoulder of $S_{\mathrm{SG/SG}}(Q)$ in this range probably arises from correlations between the N atoms, that, belonging to the SG and contributing to $S_{\mathrm{SG/SG}}(Q)$, are chemically bonded to the MC and thus also display the average periodicity of the MCs. We also note that the strong negative MC/SG-cross correlation shown in the all-atom case around $Q^{\mathrm{MC}}_{\mathrm{max}}$ (Fig. 6) disappears in the coarse-grained analysis [see Fig. 12(b)] due to the same argument. The most salient feature in the CoM cross-correlation function is a marked negative peak mirroring the main peak of the SG/SG-correlations at 1.3 Å^{-1}. This observation, together with the presence of the clear prepeak between MCs of interchain origin suggests the possibility of a domain structure constituted by side groups. A simple reason for the apparition of such a "prepeak" could be the steric hindrance of the voluminous side groups on the vinylic groups leading to an exclusion of the backbone and hence to the emergence of a prominent characteristic length in the backbone distance corresponding to $d_{\mathrm{MC}} \approx 2\pi/Q^{\mathrm{MC}}_{\mathrm{max}} = 10.5$ Å. This is a much larger distance than those usually found in simpler polymers and also than the characteristic length associated to pirrolidone rings ($d_{\mathrm{SG}} \approx 5$ Å). Finally, in the intermolecular origin of the prepeak and the intermolecular contributions to the ring

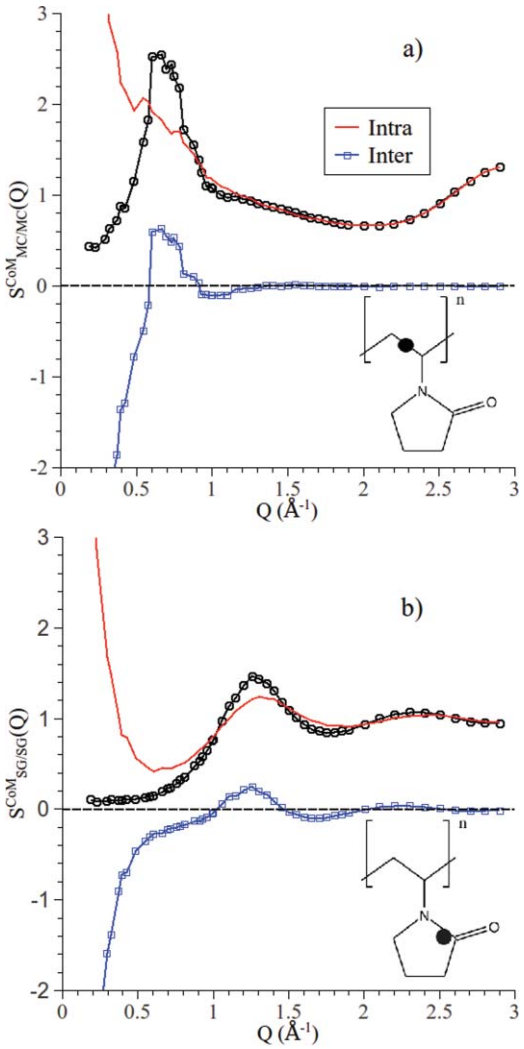

FIG. 10. (a) Structure factors (black circles) calculated for the coarse-grained system at 650 K from (a) the MC centers of mass and (b) the SG centers of mass. The intrachain contributions are plotted as red lines and the interchain contributions as blue squares and blue line. The location of the CoM in each subgroup is indicated in the respective schemes of the PVP chemical formulae.

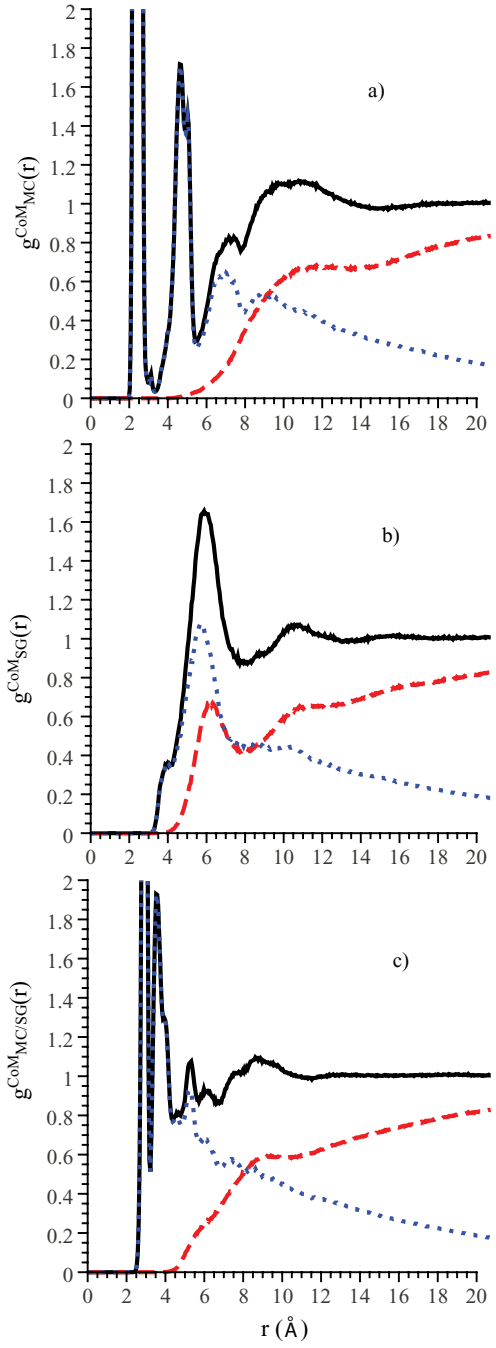

FIG. 11. Radial probability distribution functions of the MC/MC (a), SG/SG (b) and MC/SG (c) calculated from the coarse-grained simulations at 650 K. The blue dotted lines are the intrachain contributions and the red dashed lines the interchain contributions to the total (solid lines) functions. The values of $d_{MC} \approx 10$ Å and $d_{SG} = 5.5$–6 Å directly revealed agree well with those deduced from the partial structure factors analysis.

peak we can find the explanation for the temperature behavior experimentally observed in the x-ray diffraction patterns (Fig. 1).

The above scenario is supported by the radial probability distribution functions (Fig. 11). The intermolecular contribution in Fig. 11(a) directly shows that different backbones are well separated, with a first neighboring chain at around $d_{MC} \approx 10$ Å. Figure 11(b) reveals closely packed rings. Nearest neighbor rings most probably belong to consecutive monomers along one chain, but it is also rather probable to find two rings from different chains separated by a similar distance. Side groups within one chain and those in between two different chains are thus able to approach each other almost equally well ($d_{SG} = 5.5$–6 Å). At a similar distance from a ring, no backbone of another chain is expected to be found (the intermolecular MC/SG pair distribution function in Fig. 11(c) shows very small values). Thus, rings tend to be close to each other and separated from the backbones, forming domains.

2. Self-motions

The results derived for the self-motions of the CoMs are shown in Fig. 12. The left part of the figure deals with the reciprocal space analysis, while real-space magnitudes are displayed in the right part. The main differences with respect to the atomistic approach are found at microscopic times, where now the dynamics of both subgroups are indistinguishable. Moreover, in the coarse-grained approach at short-times the values of $\alpha_2^{MC}(t)$ are sensibly smaller than for $\alpha_2^{SG}(t)$, leading to different positions for both maxima. Apart from these observations, the qualitative behavior is the same for both atomistic and CoM approaches and we can state that the anomalous findings for the hydrogens are genuine and not a consequence of the particular motions developed by these specific atoms in the system. Analyzing the coarse-grained results, we have to distinguish three different regions of interest in Q:

(1) Above the main structural peak associated to SG correlations ($Q \gtrsim Q^{SG}_{max} = 1.3$ Å^{-1}), the relaxation time is independent of the nature of the relaxing units and follows a Q^{-3} law at all the temperatures investigated. The stretching parameter is around 0.3 and still insensitive to the nature of the relaxing units. The relaxation times associated to this Q region range between 10 and 200 ps for 650 K and between 1 and 10 ns for 550 K. In these time ranges the $\alpha_2(t)$ functions increase until their maximum values and $\langle r^2(t)\rangle$ display a cage rattling [Fig. 12(c)]. In the framework of the mode coupling theory (MCT), for high Q values the KWW exponent should tend to the Von Schweidler exponent $\beta(Q \to \infty) = b$ and the relaxation time dependence in this range would be $\tau(Q \to \infty) \propto Q^{-\frac{1}{b}}$, predictions compatible with our observations. This regime can be identified with the non-Gaussian regime usually observed in regular glass-forming systems at Q values larger than that corresponding to the main peak in their structure factor.

(2) In the range 0.6 Å$^{-1} \lesssim Q \lesssim 1.3$ Å^{-1}, (i.e., between Q^{MC}_{max} and Q^{SG}_{max}), a clear deviation from the previous power law can be seen for both subsystems. The characteristic times follow power laws around Q^{-2} and $Q^{-2.5}$ for SG and MC dynamics, respectively. These dependences are incompatible with a $Q^{-2/\beta}$ power law expected in the Gaussian approximation (according to the $\beta(Q)$values found [Fig. 12(a)], the Gaussian dependence would involve power laws in the range between Q^{-4} and Q^{-5}). Thus, the crossover at Q^{SG}_{max} cannot be identified

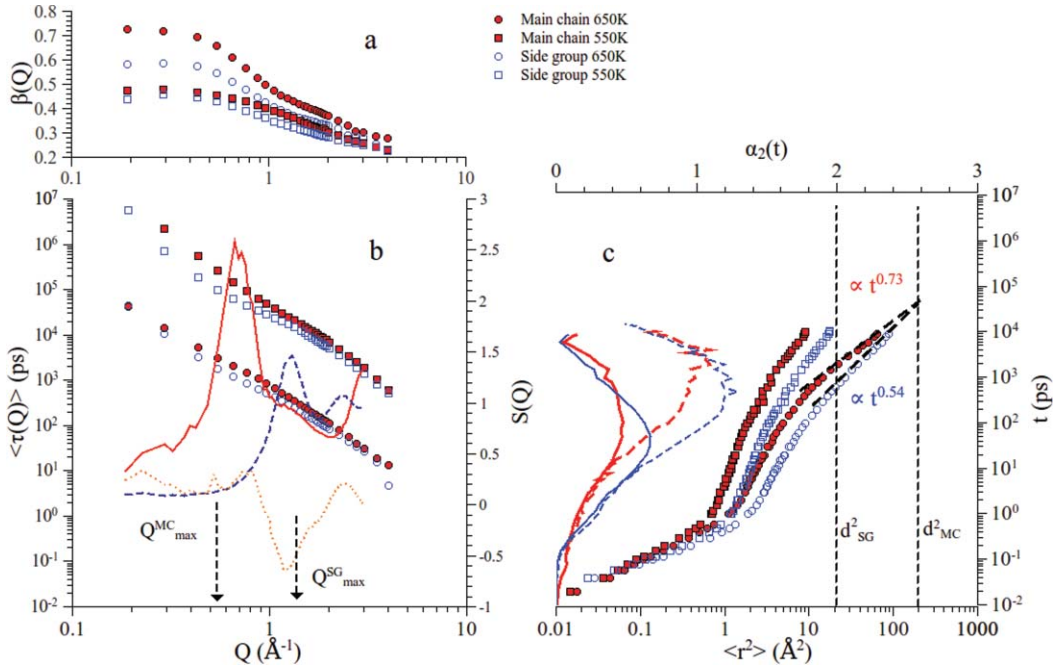

FIG. 12. Results of the coarse-grained analysis at 550 and 650 K. Fits of Eq. (11) to $F^s_{MC}(Q,t)$ and $F^s_{SG}(Q,t)$ deliver the stretching parameters and average relaxation times shown as symbols as function of Q in (a) and (b), respectively. In (b), the vertical arrows indicate the cross over between dynamical regimes, and the lines show the structure factors at 650 K (solid: MC/MC correlations; dashed: SG/SG correlations; dotted: MC/SG correlations). (c) Mean squared displacement (Filled symbols: MC; Empty symbols: SG) for the two subgroups. The non-Gaussian parameters are also shown as lines (solid for 550 K and dashed for 650 K; thin for SG and thick for MC). The time scale on the ordinate axis is the same as in (b). The dashed vertical lines mark the values corresponding to $d^2_{SG} = 23$ Å^2 and $d^2_{MC} = 110$ Å^2.

with the usual crossover Gaussian/non-Gaussian behavior observed in chemically more simple polymers.

(3) Below Q^{MC}_{max}, the β parameter reaches approximately constant values and the characteristic times of MC and SG tend to converge in a Gaussian regime. This is best seen for the highest temperature. At Q^{MC}_{max}, the values of $\langle\tau\rangle$ are 2 ns for SG and near 3 ns for MC dynamics. For both subsystems, $\alpha_2(t \gtrsim \langle\tau(Q^{MC}_{max})\rangle) \lesssim 0.2$, i.e., $G_s(r,t)$ is expected to be Gaussian. According to this observation, the SG characteristic time displays a Q^{-3} dependence and that for MC displays the continuous $Q^{-2.5}$ law started at Q^{SG}_{max}. Taking into account the corresponding β values at 650 K in this Q range, they reflect an approximately Gaussian behavior. The $\langle r^2(t)\rangle$ of MC and SG subgroups seem also to converge in this dynamical range. A similar behavior is found for the lowest temperature investigated, 550 K. There, the characteristic times at Q^{MC}_{max} are much longer (about hundreds of nanoseconds) and we cannot access the values of $\alpha_2(t = \langle\tau(Q^{MC}_{max})\rangle)$ with our simulations. However, we could expect from the extrapolations that α_2 would also be $\lesssim$0.2 above $\approx$100 ns. Also for this temperature, the deduced timescales for both, MC and SG dynamics, seem to approach each other at length scales beyond the intermain-chain characteristic distances. Hence, in this polymer two dynamical cross-overs can be identified, if the behaviors of $\tau(Q)$ above the main structural peak and below the prepeak are interpreted in the framework of a non-Gaussian to Gaussian cross-over. The dynamical behavior at intermediate scales between Q^{MC}_{max} and Q^{SG}_{max} is certainly peculiar and absent in regular polymers.

From the magnitudes in real space [Fig. 12(c)] we see that at 650 K the extrapolated $\langle r^2(t)\rangle$ of the two species would meet at a time of about 40 ns, just when they reach the value of d^2_{MC}. The characteristic times would also be expected to converge beyond this time. On the other hand, $\langle r^2_{SG}(t)\rangle$ reaches the average distance between SGs, d_{SG}, at 600 ps. At this time the dynamics is markedly heterogeneous: the main chains show much smaller displacements and move as far as the typical side-group distance only at about 2 ns. The shift of the maximum of α_2^{MC} with respect to that of the SGs indicates that the decaging of the SGs starts before the backbones can escape from their respective cages. We also note the higher values of $\alpha_2(t)$ for SG dynamics than for MC dynamics below $\approx$1 ns.

3. Collective dynamics

Valuable information can also be obtained by studying the collective dynamics through the dynamic structure factors. For different Q values, Fig. 13 shows $F^{MC}_{coh}(Q,t)$ and $F^{SG}_{coh}(Q,t)$ calculated from Eqs. (9) and (10) where α: MC-CoM and SG-CoM, respectively. While $F^{MC}_{coh}(Q,t)$ can be described by the typical KWW function [Eq. (11)], $F^{SG}_{coh}(Q,t)$ shows a progressive change in the shape of the relaxation function. For low Q values, the relaxation functional form is similar to a KWW. However, at high Q, $F^{SG}_{coh}(Q,t)$

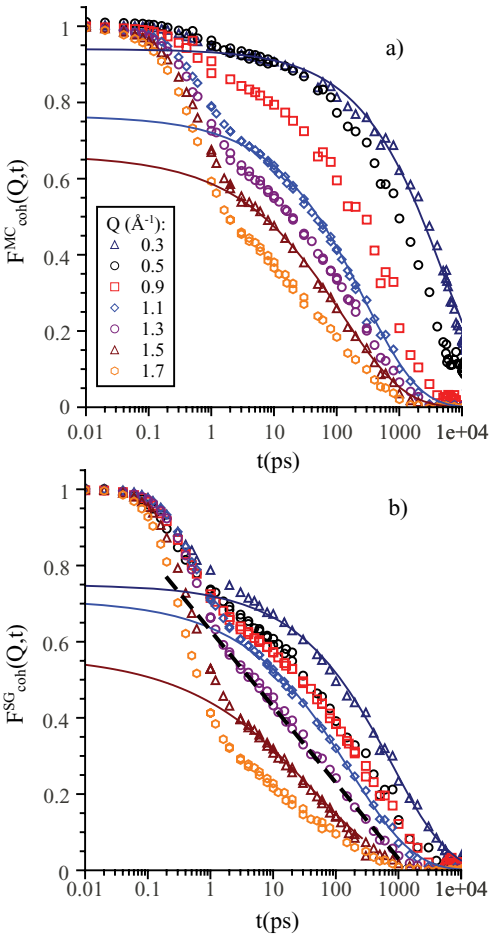

FIG. 13. (a) Coherent intermediate scattering function of the coarse-grained system for different Q values at 650 K for (a) main-chain center of mass (b) side-groups center of mass. The solid lines show KWW descriptions for selected Q values.

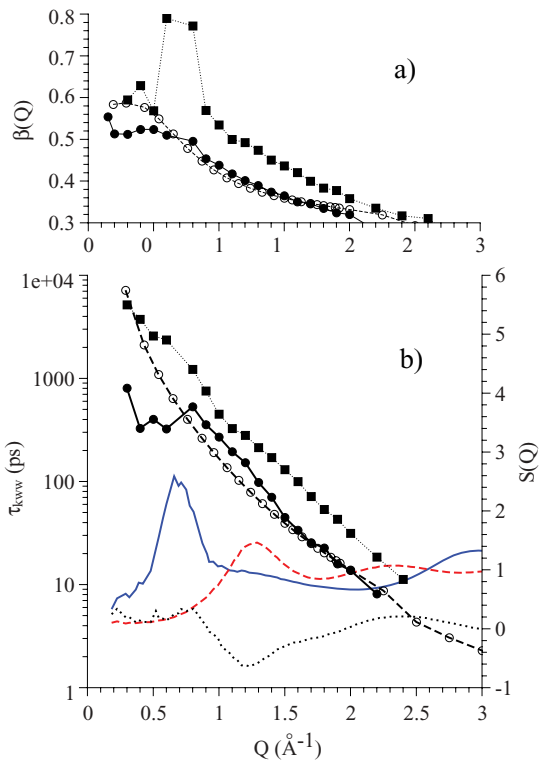

FIG. 14. Q dependence of the parameters of the KWW functions fitting the coherent intermediate scattering functions in the coarse-grained analysis at 650 K: (a) stretching parameter (b) KWW characteristic time. Full squares represent the MC subsystem, full circles the SG subsystem. The results for the self-correlation function of SG center of mass are also shown as empty circles for comparison. In (b), lines show $S^{CoM}_{MC/MC}(Q)$ (solid blue), $S^{CoM}_{SG/SG}(Q)$ (dashed red), and $S^{CoM}_{MC/SG}(Q)$ (dotted black).

exhibits an extremely extended tail, leading to a concave shape which can be effectively described with very small values of β. Around 1.5 Å^{-1}, an almost logarithmiclike relaxation is observed upon 3 decades, which is not the usually expected functional form for density correlators in glass-forming polymer systems.[55–57]

Another peculiar observation from Fig. 13 is the big difference between the characteristic times of $F^{SG}_{coh}(Q,t)$ and $F^{MC}_{coh}(Q,t)$ for small Q values. The most relevant relaxation time in a system is the structural relaxation time τ_s, i.e., the characteristic time of the dynamic structure factor at the intermolecular peak. In our system, we can find two structural relaxation times, corresponding to each of the subsystems. At 650 K, $\tau_s^{MC} = 3$ ns and $\tau_s^{SG} = 100$ ps. This implies the presence of a very large dynamic asymmetry in PVP.

The results of a KWW analysis of the coherent and incoherent intermediate scattering functions for the center of mass of side groups $F^{SG}_{coh}(Q,t)$ and $F^{SG}_{s}(Q,t)$ are shown in Fig. 14. We note in passing that there is no general theoretical predictions about the relationship between self and collective dynamics in complex systems. For simple monoatomic liquids, the coherent scattering function can be easily built starting from the incoherent one, via the so called de Gennes narrowing[58] that relates the characteristic times

$$\tau_{coh}(Q) = S(Q)\tau_{inc}(Q) \tag{14}$$

Other approximations like, e.g., that by Vineyard[59] or by Sköld[60] have been proposed as improvements of de Gennes' approach and applied also to monoatomic liquids. For stretched exponentials representing anomalous diffusion, a generalization of the de Gennes narrowing can be deduced assuming the Gaussian approximation for the incoherent scattering function:[61]

$$\tau_{coh}(Q) = S(Q)^{1/\beta}\tau_{inc}(Q). \tag{15}$$

Since the proposed approaches invoke in general some kind of modulation of the collective characteristic times with the structure factor, we have also plotted in Fig. 14(b) the partial structure factors obtained for the analysis of the CoM of each species. At high Qs (above $Q \approx 1.3$ Å^{-1}), no coherency effects are noticeable, so collective and self-relaxations are roughly the same. For smaller Q values, the relaxation times of collective motions become slightly slower (a factor $\approx$ 1.5) than self-relaxation times. This observation holds until a value limit $Q \approx 0.6$ Å^{-1}. Below this point, $\tau_{coh}(Q)$ become suddenly shorter than $\tau_{inc}(Q)$. The SG/SG structure factor presents values smaller than one for $Q \lesssim 1.1$ Å^{-1} and there a de Gennes-like narrowing would imply $\tau_{coh} < \tau_{inc}$. This is obviously not fulfilled for $0.6 \lesssim Q \lesssim 1.1$ Å^{-1}. A de Gennes narrowinglike effect can thus be discarded for SG dynamics.

The decoupling between self and collective dynamics in the SG dynamics appears between $\approx Q_{\max}^{MC} = 0.6$ Å^{-1} and $\approx Q_{\max}^{SG} = 1.3$ Å^{-1}, where the negative MC/SG-cross correlations become important. We can tentatively explain this decoupling invoking the suggested nanosegregated structure and dynamic heterogeneity between MC and SGs. Within the SG-domains, the self-dynamics of the side groups allows the local structure to relax. However, to perform a collective relaxation, the domains have to relax and vanish, which would happen only when the larger scale (backbone interchain) structure relaxes. In fact, $\tau_s^{SG}(650\ K) = 100$ ps is located in the region of the maximum of $\alpha_2^{MC}(t)$ corresponding to the decaging of the MC-CoMs [Fig. 12(c)]. We note another anomalous feature for SG-dynamics in this regime, namely that $\alpha_2^{SG}(t = \tau_s^{SG})$ presents rather high values, in contraposition to regular glass-forming polymers. The self-motions are usually Gaussian at τ_s[23], as it is also the case of the MC-subsystem: $\alpha_2^{MC}(t = \tau_s^{MC}) < 0.2$ [Fig. 12(c)].

4. Summary

The structural analysis both in real and reciprocal space point to nanosegregation and existence of ring domains. Two relevant length scales emerge, associated to the two peaks corresponding to MC/MC intermolecular correlations $Q_{\max}^{MC}$ and that of SG/SG correlations $Q_{\max}^{SG}$.

The study of the self-motions of the subsystems reveal two dynamic crossovers. Above $Q_{\max}^{SG}$, the regime characteristic for the non-Gaussian events within the cage takes place. Below $Q_{\max}^{MC}$, a Gaussian regime is found. The dynamics in the region between $Q_{\max}^{MC}$ and $Q_{\max}^{SG}$ is peculiar and absent in regular polymers. There is a delay of the MC-decaging with respect to the SGs. In this decaging time range, the dynamics of both subsystems are markedly heterogeneous and SGs show much larger deviations from Gaussian behavior than MCs. The dynamics become totally homogeneous only at much later times, when the displacements reach the average distance between main chains.

The collective dynamics study has shown a large difference in the structural relaxation times for both subsystems, i.e., a large dynamic asymmetry. $F_{coh}^{SG}(Q,t)$ shows anomalous functional form, exhibiting logarithmiclike decays close to $Q_{\max}^{SG}$. A deGennes-like relation does not hold for SG collective and self-dynamics, and they decouple between $Q_{\max}^{MC}$ and $Q_{\max}^{SG}$. Another remarkable peculiarity of SG dynamics is that at τ_s^{SG} the self-motions are markedly non-Gaussian, in contraposition to regular polymers and the MC subsystem.

V. CONNECTION WITH OBSERVATIONS IN THE LITERATURE

Logarithmic relaxations have been recently reported in different systems where dynamical heterogeneities are important. We can cite simulation works like e.g., binary mixtures of large and small spheres,[56] polymer blends with dynamical asymmetry,[62] and simulations of kinetically constrained models.[63] In the latter, slow components can relax only if the direct neighboring permits it, and their behavior is close to that observed in binary mixtures with moderate asymmetry.[56] Logarithmic relaxations are also found experimentally for side-group dynamics of poly(*n*-alkylmethacrylate) homopolymers, where a strong decoupling between self and collective dynamics also appears,[4] for mixtures of polymers with plasticizer[64] and even for hydrated proteins.[65] Another interesting comparison can be found in MD simulations of sodium disilicate,[66,67] where the following peculiar features were found: (i) a prepeak in the structure factor corresponding to preferential interactions between Na atoms and strong exclusions between Na and Si (ii) a dynamical decoupling between slow silica matrix dynamics and fast atoms of sodium (iii) the characteristic times for self-dynamics of sodium atoms show three different power laws as function of Q. The crossovers between the power laws occur at the main peak and the prepeak and finally (iv) the coincidence of the β parameter of the fast particles with the Von Schweidler exponent for high Q values. Some of those effects are strikingly similar to our observations in PVP. However, it has to be noted that in our case a true chemical bonding takes place between the subgroups, and so the existing dynamical asymmetry can only be transient in space and time. This is evidenced by Figs. 9 and 12, where at long times the $\langle r^2(t)\rangle$ of both subgroups tend to the same limit and so the characteristic times for self-relaxation of subgroups would converge at low Q values toward the beginning of the Rouse regime.

The peculiarities observed in PVP dynamics could arise from more general theoretical considerations. In some of the previously cited works, the observed dynamical decoupling and logarithmic decay of intermediate scattering functions are tentatively interpreted in the framework of a higher order MCT transition[55,57,68,69] that arises when two (or more[70]) different dynamical arrest processes occur. For PVP side groups, they could be bulklike caging, common to all glass formers, and a "soft caging" induced by the polymer backbone. Also two different relevant length scales can be invoked to generate a higher order MCT transition. In the case of PVP, they would be that associated to the main-chain/main-chain correlations ($d_{MC} \approx 10$ Å) and the other one to the average distances between side groups ($d_{SG} \approx 5$ Å).

This scenario may also help to understand the suspected existence of two different structural relaxation arrests at respectively 323 and 440 K by Karabanova *et al.*[16,17] From dielectric experiments by Cerveny *et al.*,[71] two main relaxation peaks were reported. That measured at lower frequencies is assigned to an $\alpha\beta$ process at high temperature that splits into an α and a β process around 475 K. Below this temperature, only the β process can be probed by dielectric spectroscopy. Another faster process called γ is detected as a peak at high frequencies in the dielectric signal and is assigned to a local relaxation. The γ relaxation frequency is about 10 Hz around 320 K. At this temperature Karabanova *et al.* have detected by dynamical mechanic spectroscopy (around 10 Hz) a relaxation process that they have assigned to a second glass transition.[16] Combining the results of the previous experiments with ours, we propose the following scenario based on a decoupling between backbone dynamics and SGs dynamics that seems to become stronger as the temperature decreases (see Fig. 12). In the highest temperatures studied by dielectric relaxation and dynamic mechanical analysis (around 445

K) those results would reflect the structural relaxation of the slower subsystem, hence the backbone structural relaxation. The vanishing of the α relaxation (and the raise of the β process) probed by dielectric spectroscopy could be explained by the weakness of the dipole in the vinylic backbone. However, as the backbone is linked to a nitrogen atom belonging to the SG, which has a dipolar moment, a local dipole between backbone and pyrrolidone ring may exist. Hence the β process detected by dielectric spectroscopy can be understood as a local reorganization of this dipole between the backbone and the nitrogen of pyrrolidone ring. The γ relaxation of Cerveny *et al.* could be in this framework the structural relaxation of the pyrrolidone rings inside their rich domains that would be completely decoupled from the (frozen) backbone dynamics in the low temperature region. The arrest for this structural relaxation involving the ring domains structure would occur around 320 K, as probed by dielectric spectroscopy and dynamic mechanical analysis. A similar situation could apply to the case of poly (isobornyl methacrylate).[15]

VI. SUMMARY AND CONCLUSIONS

We have carried out scattering experiments and MD simulations on PVP. The good agreement between simulations and experiments, upon structure and dynamics, validates the simulations that have been further exploited to gain a more detailed insight. Analyzing the self-dynamics of main chains and side groups, we have shown that both high Q and low Q limits of $F_s(Q,t)$ can be understood in the framework of a non-Gaussian to Gaussian cross over. However, in contraposition to regular glass-forming polymers, a third dynamical regime appears at intermediate Q values. This regime is found in both, hydrogens and centers of mass analysis, and extends between the prepeak in the structure factor around 0.6 Å^{-1} (that can be identified with main-chain/main-chain correlations), and the main peak characteristic for side-groups/side groups correlations around 1.3 Å^{-1}. In this intermediate regime, the dynamics of main chains and side groups are decoupled. As a consequence, both subgroups perform quasi-independent dynamics in a defined space and time range leading to two different structural relaxations. Logarithmic decays in the density–density correlator and unusually large deviations from Gaussianity at the structural relaxation time of the fastest subgroup (the side groups) emerge. Similar behavior has been found in simulations of binary mixtures with marked dynamical asymmetry. For PVP side groups, we speculate that abnormal relaxation processes could be understood in the framework of the MCT by the presence of two different dynamical arrest mechanisms: first, a normal caging regime due to the direct neighbors of the side-groups domains and second a "soft caging" regime driven by the polymer backbone relaxations. As the subgroups are chemically bonded, a correlation between both subsystems takes place and motions cannot be totally decoupled at long times/large length scales. Therefore, at low-Q values a Gaussian crossover takes place or, simply speaking, a recorrelation appends toward the Rouse regime. Thus, we have shown that some anomalous dynamics relaxation and nanosegregation effects could be identified not only in polymers with long alkyl side chains as poly-*n*-alkyl-methacrylates, poly-*n*-alkyl-acrylates, and poly-di-*n*-alkyl-itaconates, but also in polymers owning shorter and *intrinsically* simple side groups.

ACKNOWLEDGMENTS

We want to thank A. Moreno for stimulating and fruitful discussions and J-M. Zanotti for development of QENSH software data treatment. We acknowledge support by the DIPC, the European Commission NoE SoftComp, Contract NMP3-CT-2004-502235, the projects MAT2007-63681, IT-436-07 (GV), and the Spanish Ministerio de Educacion y Ciencia (Grant No. CSD2006-53).

[1] J. J. d. Val, A. Alegria, J. Colmenero, C. Mijangos, G. Martinez, and J. LuisMillan, Die Makromol. Chem. **190**, 3257 (1989).
[2] M. Beiner, Macromol. Rapid Commun. **22**, 869 (2001).
[3] C. Gerstl, G. J. Schneider, W. Pyckhout-Hintzen, J. Allgaier, D. Richter, A. Alegria, and J. Colmenero, Macromolecules **43**, 4968 (2010).
[4] A. Arbe, A.-C. Genix, S. Arrese-Igor, J. Colmenero, and D. Richter, Macromolecules **43**, 3107 (2010).
[5] A.-C. Genix, A. Arbe, F. Alvarez, J. Colmenero, B. Farago, A. Wischnewski, and D. Richter, Macromolecules **39**, 6260 (2006).
[6] A.-C. Genix, A. Arbe, F. Alvarez, J. Colmenero, W. Schweika, and D. Richter, Macromolecules **39**, 3947 (2006).
[7] E. Dudognon, A. Bernès, and C. Lacabanne, Macromolecules **35**, 5927 (2002).
[8] E. Dudognon, A. Bernès, and C. Lacabanne, Macromolecules **34**, 3988 (2001).
[9] M. Beiner, K. Schroter, E. Hempel, S. Reissig, and E. Donth, Macromolecules **32**, 6278 (1999).
[10] M. Beiner, O. Kabisch, S. Reichl, and H. Huth, J. Non-Cryst. Solids **307-310**, 658 (2002).
[11] M. Beiner and H. Huth, Nature Mater. **2**, 595 (2003)
[12] M. Wind, R. Graf, S. Renker, H. W. Spiess, and W. Steffen, J. Chem. Phys. **122**, 014906 (2005).
[13] A. Arbe, A. C. Genix, J. Colmenero, D. Richter, and P. Fouquet, Soft Matter **4**, 1792 (2008).
[14] S. Hiller, O. Pascui, H. Budde, O. Kabisch, D. Reichert, and M. Beiner, New J. Phys. **6**, 10 (2004).
[15] F. Alvarez, J. Colmenero, C. H. Wang, J. L. Xia, and G. Fytas, Macromolecules **28**, 6488 (1995).
[16] L. V. Karabanova, G. Boiteux, O. Gain, G. Seytre, L. M. Sergeeva, and E. D. Lutsyk, J. Appl. Polym. Sci. **80**, 852 (2001).
[17] L. V. Karabanova, G. Boiteux, O. Gain, G. Seytre, L. M. Sergeeva, E. D. Lutsyk, and P. A. Bondarenko, J. Appl. Polym. Sci. **90**, 1191 (2003).
[18] S. W. Lovesey, *Theory of Neutron Scattering from Condensed matter* (Oxford University Press, Oxford, 1971).
[19] B. Frick and M. Gonzalez, Physica B **301**, 8 (2001).
[20] H. Sun, J. Phys. Chem. B **102**, 7338 (1998).
[21] H. Sun, P. Ren, and J. R. Fried, Comput. Theor. Polym. Sci. **8**, 229 (1998).
[22] A. Arbe, J. Colmenero, F. Alvarez, M. Monkenbusch, D. Richter, B. Farago, and B. Frick, Phys. Rev. Lett. **89**, 245701 (2002).
[23] J. Colmenero, F. Alvarez, and A. Arbe, Phys. Rev. E **65**, 41804 (2002).
[24] A.-C. Genix, A. Arbe, F. Alvarez, J. Colmenero, L. Willner, and D. Richter, Phys. Rev. E **72**, 031808 (2005).
[25] D. N. Theodorou and U. W. Suter, Macromolecules **19**, 139 (1986).
[26] D. N. Theodorou and U. W. Suter, Macromolecules **19**, 379 (1986).
[27] L. Van Hove, Phys. Rev. **95**, 249 (1954).
[28] A. Rahman, K. S. Singwi, and A. Sjölander, Phys. Rev. **126**, 986 (1962).
[29] P. A. Doyle and P. S. Turner, Acta Crystallogr., Sect. A: Found. Crystallogr. **24**, 390 (1968).
[30] B. Frick, D. Richter, and Cl. Ritter, Europhys. Lett. **9**, 557 (1989).
[31] R. Pérez-Aparicio, A. Arbe, F. Alvarez, J. Colmenero, and L. Willner, Macromolecules **42**, 8271 (2009).
[32] J. Colmenero, A. Arbe, and A. Alegría, Phys. Rev. Lett. **71**, 2603 (1993).
[33] D. Richter, M. Monkenbusch, A. Arbe, J. Colmenero, *Neutron Spin Echo in Polymer Systems* (Springer-Verlag, Berlin, Heidelberg, 2005).

[34]A. Arbe, D. Richter, J. Colmenero, and B. Farago, Phys. Rev. E **54**, 3853 (1996).
[35]A. Narros, A. Arbe, F. Alvarez, J. Colmenero, and D. Richter , J. Chem. Phys. **128**, 224905 (2008).
[36]A. Arbe, J. Colmenero, M. Monkenbusch, and D. Richter, Phys. Rev. Lett. **82**, 1336 (1998).
[37]J. Sacristan, F. Alvarez, and J. Colmenero, Eur. Phys. Lett. **80**, 38001 (2007).
[38]B. Vorselaars, A. V. Lyulin, K. Karatasos, and M. A. J. Michels, Phys. Rev. E **75**, 011504 (2007).
[39]J. Wuttke, I. Chang, O. G. Randl, F. Fujara, and W. Petry, Phys. Rev. E **54**, 5364(1996).
[40]R. Busselez, R. Lefort, M. Guendouz, B. Frick, O. Merdrignac-Conanec, and D. Morineau, J. Chem. Phys. **130**, 214502 (2009).
[41]J. Colmenero, A. Alegría, A. Arbe, and B. Frick, Phys. Rev. Lett. **69**, 478 (1992).
[42]S. Mossa, R. Di Leonardo, G. Ruocco, and M. Sampoli, Phys. Rev. E **62**, 612 (2000).
[43]A. Arbe, J. Colmenero, F. Alvarez, M. Monkenbusch, D. Richter, B. Farago, and B. Frick, Phys. Rev. E **67**, 51802 (2003).
[44]A. Soldera and Y. Grohens, Polymer **45**, 1307 (2004).
[45]M. Tyagi, A. Arbe, F. Alvarez, J. Colmenero, and M. A. Gonzalez, J. Chem. Phys. **129**, 224903 (2008).
[46]S. Capponi, A. Arbe, F. Alvarez, J. Colmenero, B. Frick, and J. P. Embs, J. Chem. Phys. **131**, 204901 (2009).
[47]G. D. Smith, W. Paul, M. Monkenbusch, L. Willner, D. Richter, X. H. Qiu, and M. D. Ediger, Macromolecules **32**, 8857 (1999).
[48]See supplementary material at http://dx.doi.org/10.1063/1.3533771 for the comparison between the characteristic times obtained from simulations and QENS.
[49]This function would be to a good approximation proportional to the coherent cross section accessed by neutron diffraction on a fully deuterated sample.
[50]R. L. Miller, R. F. Boyer, and J. Heijboer, J. Polym. Sci., Polym. Phys. Ed. **22**, 2021 (1984).
[51]G. Floudas and P. Stepanek, Macromolecules **31**, 6951 (1998).
[52]M. Gaborieau, R. Graf, S. Kahle, T. Pakula, and H. W. Spiess, Macromolecules **40**, 6249 (2007).
[53]V. Arrighi, P. F. Holmes, I. J. McEwen, H. Qian, and N. J. Terrill, J. Polym. Sci., Part B: Polym. Phys. **42**, 4000 (2004).
[54]V. Arrighi, A. Triolo, I. J. McEwen, P. Holmes, R. Triolo, and H. Amenitsch, Macromolecules **33**, 4989 (2000).
[55]W. Götze and M. Sperl, Phys. Rev. E **66**, 011405 (2002).
[56]A. J. Moreno and J. Colmenero, J. Chem. Phys. **125**, 164507 (2006).
[57]A. J. Moreno and J. Colmenero, J. Chem. Phys. **124**, 184906 (2006).
[58]P. G. De Gennes, Physica **25**, 825 (1959).
[59]G. H. Vineyard, Phys. Rev. **110**, 999 (1958).
[60]K. Sköld, Phys. Rev. Lett. **19**, 1023 (1967).
[61]A. Arbe, J. Colmenero, and D. Richter, *Broad band dielectric spectroscopy* (Springer-Verlag, Heidelberg, 2002) pp. 685–718.
[62]A. J. Moreno and J. Colmenero, Phys. Rev. Lett. **100**, 126001 (2008).
[63]A. J. Moreno and J. Colmenero, J. Chem. Phys. **125**, 016101 (2006).
[64]D. Bingemann, N. Wirth, J. Gmeiner, and E. A. Rössler, Macromolecules **40**, 5379 (2007).
[65]X.-q Chu, M. Lagi, E. Mamontov, E. Fratini, P. Baglioni, and S.-H. Chen, Soft Matter **6**, 2623 (2010).
[66]J. Horbach, W. Kob, and K. Binder, Phys. Rev. Lett. **88**, 125502 (2002).
[67]A. Meyer, J. Horbach, W. Kob, F. Kargl, and H. Schober, Phys. Rev. Lett. **93**, 027801 (2004).
[68]V. Krakoviack, Phys. Rev. Lett. **94**, 065703 (2005).
[69]V. Krakoviack, Phys. Rev. E **79**, 061501 (2009).
[70]F. Sciortino, P. Tartaglia, and E. Zaccarelli, Phys. Rev. Lett. **91**, 268301 (2003).
[71]S. Cerveny, A. Alegria, and J. Colmenero, J. Chem. Phys. **128**, 44901 (2008).